Manuscript prepared for Atmos. Meas. Tech. Discuss.
with version 4.1 of the LaTeX class copernicus_discussions.cls.
Date: 2 December 2014

Observing crosswind over urban terrain using scintillometer and Doppler lidar

D. van Dinther[1], C. R. Wood[2], O. K. Hartogensis[1], A. Nordbo[3], and E. J. O'Connor[2,4]

[1]Wageningen University, Meteorology and Air Quality Group, Wageningen, the Netherlands
[2]Finnish Meteorological Institute, Helsinki, Finland
[3]University of Helsinki, Department of Physics, Helsinki, Finland
[4]University of Reading, Department of Meteorology, Reading, United Kingdom

Correspondence to: D. van Dinther
(danielle.vandinther@wur.nl)

Abstract

In this study, the crosswind (wind component perpendicular to a path, $U_\perp$) ~~is~~ has been measured by a scintillometer and Doppler lidar above the urban environment of Helsinki, Finland, for ~~3 weeks~~15 days. The scintillometer allows acquisition of a path-averaged value of $U_\perp$ ($\overline{U_\perp}$), while the Doppler lidar allows acquisition of path-resolved $U_\perp$ ($U_\perp(x)$, where x is the position along the path). The goal of this study is to evaluate the ~~applicability~~ performance of scintillometer $\overline{U_\perp}$ ~~measurements~~ -estimates for conditions where $U_\perp(x)$ is variable. ~~If the scintillometer is applicable in such variable-wind conditions, it can also be used in the urban environment.~~ Two methods were applied to obtain $\overline{U_\perp}$ from the scintillometer signal; the cumulative spectrum method (relies on scintillation spectra) ~~,~~ and the lookup table method (relies on time-lagged correlation functions). ~~Both~~ The values of $\overline{U_\perp}$ of both methods compared reasonably well with the Doppler lidar ~~measurements, especially considering the challenging urban environment in which they were measuring; with RMSE~~ estimates; with root mean square errors of 0.71 and 0.73 m s^{-1}. This indicates that, given the data treatment applied in this study, both measurement technologies are able to obtain $\overline{U_\perp}$ in the complex urban environment. The ~~in detail~~ detailed investigation of four cases indicate that the cumulative spectrum method is less susceptible to a variable $U_\perp(x)$ than the lookup table method. However, the lookup table method can be adjusted to improve its capabilities to obtain $\overline{U_\perp}$ for conditions where $U_\perp(x)$ is variable.

1 Introduction

The general application of a scintillometer in micrometeorology is obtaining path-averaged surface fluxes (among others De Bruin, 2002; Meijninger et al., 2002a,b). The path can range from a few hundred meters to a few kilometers depending on the type of scintillometer used (De Bruin, 2002). In this study the focus is on ~~another application of scintillometers, which is~~ obtaining the path-averaged crosswind from a scintillometer (among others Briggs et al., 1950; Wang et al., 1981), where the crosswind ($U_\perp$) is defined as the wind-component perpendicular to ~~a~~ the scintillometer path. By obtaining a path-averaged value of $U_\perp$ ($\overline{U_\perp}$) instead of a point measurement, a scintillometer is more suitable for validation of winds from model output – given the resolution of numerical weather prediction models (~10 km) – than point

measurements. Furthermore, in the roughness sublayer, due to ground clutter point measurements can more easily be biased than path-averaged values.

From scintillometer data, one can obtain $\overline{U_\perp}$ from either the scintillation power spectrum ($S_{11}(f)$, where f is the frequency) (van Dinther et al., 2013) or the time-lagged correlation function ($r_{12}(\tau)$, where τ is the time-lag) (among others Briggs et al., 1950; Poggio et al., 2000; van Dinther and Hartogensis, 2014). The validation of $\overline{U_\perp}$ ~~scintillometer measurements~~ has, so far, mainly taken place on flat grassland sites (Poggio et al., 2000; van Dinther et al., 2013). ~~On these~~ At such sites $U_\perp$ is assumed to be uniform along the scintillometer path. ~~However~~Despite that, there is also a need for scintillometer $\overline{U_\perp}$ in more complex areas, such as mountain environments (Poggio et al., 2000) and urban environments (Wood et al., 2013c). Ward et al. (2011) studied the influence of a variable $U_\perp$-field along the path ($U_\perp(x)$, where x is the location on the scintillometer path) on the scintillometer signal – however, their focus was on scintillation spectra and structure parameter ~~measurements~~ estimates rather than on $\overline{U_\perp}$~~-measurements~~-estimates. The $U_\perp(x)$-fields used in their study were all synthetic. In the present study, the focus is on the influence of a measured (i.e., non-synthetic) variable $U_\perp(x)$ on the $\overline{U_\perp}$~~-measurement~~-estimate of a scintillometer.

The measurements investigated in this study are taken in the urban environment. In such an environment the wind speed and direction ~~is~~ are spatially variable (Bornstein and Johnson, 1977), making it a suitable environment to study the influence of a variable $U_\perp(x)$ on the scintillometer ~~measurements~~ estimates of $\overline{U_\perp}$. Key to this study ~~is~~ are measurements of the variability of $U_\perp(x)$, that are estimated by a scanning Doppler lidar (LIght Detection And Ranging). In this experiment the Doppler lidar was set up in a horizontal scan configuration, in order to estimate the horizontal wind speed and wind direction along the scintillometer path using a duo-beam method as was done in Wood et al. (2013c) above the River Thames in London.

The measurements were taken in Helsinki, Finland, as part of the Helsinki Urban Boundary-Layer Atmosphere Network (Wood et al., 2013a). The strong spatial and temporal variability of $U_\perp(x)$ induced by buildings poses challenges for both the Doppler lidar and the scintillometer technologies: (i) the Doppler lidar, since one assumes homogeneity of the wind field within each range-gate (sampling bin) for both beams: and (ii) the scintillometer, since both $S_{11}(f)$ and $r_{12}(\tau)$ used in the $\overline{U_\perp}$-retrieval algorithms, are influenced by a variable $U_\perp(x)$ although the algorithms do not take this influence into account (van Dinther et al., 2013; van

Dinther and Hartogensis, 2014). We are, therefore, working at the limit of both measurement technologies.

The main goal of this study is to investigate the performance of the scintillometer to measure $\overline{U_\perp}$ in conditions where $U_\perp(x)$ is variable. In order to do so, ~~firstly the~~ scintillometer estimates of $\overline{U_\perp}$ are compared to estimates that of the Doppler lidar. However, also for the Doppler lidar the heterogeneous wind conditions are challenging. Therefore, before the scintillometer and Doppler lidar $\overline{U_\perp}$ estimates are compared to each other the applicability of the Doppler lidar to estimate $U_\perp(x)$ ~~will be~~ is investigated by comparing with sonic anemometer measurements. ~~Secondly, the scintillometer $\overline{U_\perp}$-measurements will be validated with the Doppler lidar measurements.~~ Lastly, four cases will be selected where $U_\perp(x)$ ~~measured~~ estimated by the Doppler lidar is used to obtain the theoretical $S_{11}(f)$ and $r_{12}(\tau)$, from the models given by Clifford (1971) and Lawrence et al. (1972), respectively. The influence of a variable $U_\perp(x)$ on the theoretical $S_{11}(f)$ and $r_{12}(\tau)$ gives insight into the robustness of the scintillometer methods to obtain $\overline{U_\perp}$.

2 Theory and Methods

2.1 Scintillometry

A scintillometer consists of a transmitter and a receiver. ~~The transmitter emits light with a certain wavelength, which is refracted~~ In this study, a large aperture scintillometer is used of which the transmitter emits near-infrared radiation. This radiation is scattered by eddies in the atmosphere. The ~~eddy field in the~~ atmosphere is turbulent~~(i.e., constantly changing), therefore the receivermeasures intensity fluctuations~~ , leading to an eddy field which constantly changes. The intensity measured by the receiver, therefore, fluctuates on short time-scales ($\sim$ 1 s). ~~When~~ For these time-scales Taylor's frozen-turbulence assumption is valid, making $U_\perp$ ~~is~~ the only driver of changes in the eddy field.

The value of $\overline{U_\perp}$ can be obtained from the ~~scintillation signal~~ intensity fluctuations (also referred to as scintillation signal) by either the scintillation power spectrum or time-lagged correlation function. In this study we will use the cumulative spectrum method to obtain $\overline{U_\perp}$ from $S_{11}(f)$ (van Dinther et al., 2013), and the lookup table method to obtain $\overline{U_\perp}$ from $r_{12}(\tau)$ (van Dinther and Hartogensis, 2014).

2.1.1 ~~Scintillation spectra~~

A detailed description of ~~how $\overline{U_\perp}$ can be determined from scintillation spectra is~~ the methods are given in van Dinther et al. (2013) ~~. A~~ and van Dinther and Hartogensis (2014) , a brief outline of the ~~method is~~ methods are given below.

2.1.1 Scintillation spectra

The scintillation spectrum ($S_{11}(f)$) gives insight into which frequencies contribute to the variance of the scintillation signal. Clifford (1971) describes a theoretical model of the scintillation spectrum. Adjusting this model for a large-aperture scintillometer (as used in this study) gives (Nieveen et al., 1998):

$$S_{11}(f) = 16\pi^2 k^2 \int_0^1 \int_{2\pi f/U_\perp(x)}^{\infty} K\phi_n(K)\sin^2\left(\frac{K^2 Lx(1-x)}{2k}\right)\left[(KU_\perp(x))^2 - (2\pi f)^2\right]^{-1/2}$$
$$\left(\frac{2J_1(0.5KDx)}{0.5KDx}\frac{2J_1(0.5KD_{\mathrm{R}}x)}{0.5KD_{\mathrm{R}}x}\right)^2\left(\frac{2J_1(0.5KD(1-x))}{0.5KD(1-x)}\frac{2J_1(0.5KD_{\mathrm{T}}(1-x))}{0.5KD?\mathrm{T}(1-x)}\right)^2 dK\,dx, \quad (1)$$

where f is the frequency for which S_{11} is representative, k is the wave number of the emitted radiation, K the turbulent spatial wave number, L is the scintillometer path length, x is the relative location on the path, J_1 is the first-order Bessel function ~~, D~~ of the first kind, D_{R} is the aperture diameter of the ~~scintillometer,~~ receiver, D_{T} is the aperture diameter of the transmitter, and $\phi_n(K)$ is the three-dimensional spectrum of the refractive index in the inertial range given by Kolmogorov (1941). As can be seen in Eq. (1), $U_\perp(x)$ influences the scintillation spectrum. In fact, the scintillation spectrum shifts linearly across the frequency axis as a function of $\overline{U_\perp}$. Therefore, by obtaining a characteristic point in the spectrum, $\overline{U_\perp}$ can be obtained ~~.~~(van Dinther et al., 2013) .

The cumulative spectrum is obtained by integrating a scintillation spectrum from low to high frequency and normalizing this integration by the variance in the scintillation signal. The cumulative spectrum method takes into account multiple characteristic frequency points (f_{CS}), which are in this study defined as the frequency points where the cumulative spectrum is 0.5, 0.6, 0.7, 0.8, and 0.9 ~~. For all~~ (as in van Dinther et al. (2013)). For each of these five points, a

value of $\overline{U_\perp}$ is determined by:

$$\overline{U_\perp} = C_{\mathrm{CS}} \cdot f_{\mathrm{CS}}, \tag{2}$$

where C_{CS} is a ~~constant for which the value is determined~~ unique constant, which depends on the experimental setup and scintillometer used, that can be derived from the theoretical $S_{11}(f)$ (Eq. (1)), by filling in values of $U_\perp$ and assuming that $U_\perp(x)$ is constant, for the five different frequency points. ~~The~~ Subsequently, the five different $\overline{U_\perp}$-values are averaged to obtain one value of $\overline{U_\perp}$ per cumulative spectrum. In this study we will investigate ~~if~~ to what extend the assumption that $C_{\mathrm{CS}} =$ constant ~~also~~ holds when $U_\perp(x)$ varies. This investigation is carried out by means of four cases where the $U_\perp(x)$~~-measurements~~ -estimates of the Doppler lidar are used in Eq. (1) to obtain the theoretical $S_{11}(f)$. Therefore, Eq. (1) is not integrated for x over 0 to 1, but over the 139 range-gates measured by the Doppler lidar (see Sect. 4.3). The cumulative spectra are ~~in this study~~ obtained over 10-min periods ~~.~~ in this study.

2.1.2 Time-lagged correlation function

~~A detailed description of how $\overline{U_\perp}$ can be determined from the time-lagged correlation function is given in van Dinther and Hartogensis (2014) . A brief outline of the method is given below.~~ The value of $\overline{U_\perp}$ can be obtained from a dual-aperture scintillometer (scintillometer with ~~two spatially separated transmitters and receivers~~horizontally displaced beams) using $r_{12}(\tau)$. The benefit of the methods relying on $r_{12}(\tau)$ instead of $S_{11}(f)$ is that also the ~~sign~~ crosswind direction (i.e., the sign of $\overline{U_\perp}$) can be obtained from $r_{12}(\tau)$. Another benefit is that $r_{12}(\tau)$ can be determined over a short time-scale ($\sim$ 10 s), while $S_{11}(f)$ needs to be determined over a longer time-scale ($\sim$ 10 min). On the other hand, $r_{12}(\tau)$ needs to be obtained from a dual-aperture scintillometer, while scintillation spectra can in principal be obtained from ~~the more-widely available single-aperture scintillometers.~~ every type of scintillometer.
The crosswind transports the eddy field through the scintillometer beams. ~~When frozen turbulence is assumed, the~~ For a dual-aperture scintillometer the two transmitters and receivers are in general setup with only a small separation distance ($\sim$ 10 cm) between the two. Therefore, it takes a short time for the eddy field to travel from the one beam to the other, making that the eddy field barely changes (i.e., frozen turbulence assumption can be assumed). The signals of the two spatially separated scintillometer beams should ~~be~~ thus be almost identical except for a time shift. This time shift is related to $\overline{U_\perp}$, and can be obtained

from $r_{12}(\tau)$. A theoretical model of the time-lagged covariance function ($C_{12}(\tau)$) is given by Lawrence et al. (1972), here including the large-aperture averaging terms of Wang et al. (1978):

$$C_{12}(\tau) = 16\pi^2 k^2 \int_0^1 \int_0^\infty K\phi_n(K)\sin^2\left[\frac{K^2 Lx(1-x)}{2k}\right] J_0\{K[s(x) - U_\perp(x)\tau]\}$$

$$\left[\frac{2J_1(0.5KD_r x)}{0.5KD_r x}\,\frac{2J_1(0.5KD_{\mathsf{R}} x)}{0.5KD_{\mathsf{R}} x}\right]^2 \left\{\frac{2J_1[0.5KD_t(1-x)]}{0.5KD_t(1-x)}\,\frac{2J_1[0.5KD_{\mathsf{T}}(1-x)]}{0.5KD_{\mathsf{T}}(1-x)}\right\}^2 dK\,dx, \quad (3)$$

where J_0 is the zero-order Bessel function ~~,~~ of the first kind, and $s(x)$ is the separation distance between the two beams at location x~~on the path, D_r is the aperture diameter of the receiver, and D_t is the aperture diameter of the transmitter~~. The theoretical $r_{12}(\tau)$ can be obtained by dividing the theoretical $C_{12}(\tau)$ by the theoretical $C_{11}(\tau)$, where $C_{11}(\tau)$ is ~~given by~~ obtained from Eq. (3) by taking $s(x) = 0$ (i.e., variance of the signal).

In this study, we will use the lookup table method to obtain $\overline{U_\perp}$ from $r_{12}(\tau)$. ~~The lookup table consists~~ A lookup table is created with values of the theoretical $r_{12}(\tau)$ (using Eq. (3)) given a range of $\overline{U_\perp}$ values (resolution of 0.1 m s^{-1}) and time-lag values (resolution of 0.002 s, ~~related~~ equal to the measurement frequency of the scintillometer) (van Dinther and Hartogensis, 2014). ~~When creating the lookup table,~~ Note that $U_\perp(x)$ is assumed to be constant ~~. In order to obtain~~ when creating the lookup table. The estimate of $\overline{U_\perp}$ ~~,~~ is obtained by comparing the measured $r_{12}(\tau)$ ~~is compared~~ values to the theoretical $r_{12}(\tau)$ values ~~, given different values of $\overline{U_\perp}$, of~~ of the lookup table. The theoretical $r_{12}(\tau)$ that has the best fit with the measured $r_{12}(\tau)$ thus yields the value of $\overline{U_\perp}$.

The effects of having a variable $U_\perp(x)$ on $r_{12}(\tau)$ and thereby on $\overline{U_\perp}$ will be investigated by means of four cases (see Sect. 4.3). For these four cases Eq. (3) is integrated over the 139 ~~steps of x with~~ range gates given the different values for $U_\perp(x)$ estimated by the Doppler lidar. In this study $r_{12}(\tau)$, and thereby $\overline{U_\perp}$, are determined over 10-s intervals. For the comparison between the scintillometer and Doppler lidar the 10-s $\overline{U_\perp}$-values are arithmetically averaged to 10 min.

2.2 Doppler lidar

In this study, a HALO Photonics (Malvern, UK) Streamline scanning Doppler lidar is used. Full details of this type of Doppler lidar are described in Hirsikko et al. (2014), but briefly summarized here. The Doppler lidar emits pulses of radiation at a wavelength of 1.5 μm; any backscattered radiation from aerosols is used to estimate wind in the atmosphere by assuming that aerosols are perfect tracers of the wind. In the returned signal there is a Doppler shift, which enables calculation of the Doppler velocity, i.e., the velocity in the direction in which the Doppler lidar beam is pointing (also referred to as radial or along-beam wind). ~~However, in this study~~
In this study, the crosswind component of the wind speed is needed in order to compare with scintillometer ~~measurements, given that the Doppler lidar was located near the receiver of the scintillometer~~estimates. The required wind component can be estimated from the radial Doppler velocities by applying the duo-beam method (Wood et al., 2013c), ~~where~~ which determines the horizontal wind speed and wind direction ~~can be estimated from the Doppler lidar measurements~~ using trigonometric identities, from which $U_{\perp}(x)$ can be determined. The duo-beam method relies, as the name implies, on two sets of measurements from the Doppler lidar: at two different azimuths (i.e., beam-pointing directions in the horizontal plane). A detailed description of this method is given in Wood et al. (2013c), a brief outline of the method is given here. The radial velocity (V_b^g) for each range-gate (g), as ~~measured~~ estimated by the Doppler lidar, and beam angle (b) is given by

$$V_b^g = U^g \cos(\phi^g + \pi - \theta_b), \tag{4}$$

where U^g is the transect wind speed, ϕ^g is the wind-direction bearing from north, and θ_b is the bearing of the beam angle. When applying Eq. (4) for two beams, with different θ_b, the two unknowns U^g and ϕ^g can be solved, by assuming $V_1^g = V_2^g$. From U^g and ϕ^g, the value of $U_{\perp}$ can be obtained for each range gate. It is implicit in this method that the wind field is constant between the two lidar beams. Clearly this is not the case in the atmosphere, and one might expect the effects to average out above the roughness sublayer. But in the roughness sublayer there will inevitably be error, perhaps including bias, caused by this implicit assumption.

3 Experimental setup

The measurements were conducted in Helsinki, Finland, as part of the Helsinki Urban Boundary-Layer Atmosphere Network (Wood et al., 2013a, http://urban.fmi.fi). The measurements in the present study were taken from ~~the~~ 1st to ~~the~~ 15th of October 2013. The measurement devices used in this study are a scintillometer, a Doppler lidar, and two sonic anemometers. A layout of the measurement devices is given in Fig. 1.

The scintillometer used in this study is a BLS900 ~~of Scintec (~~(Scintec, Rottenburg, Germany) running with SRun software version 1.09. Note that in this study the output of $\overline{U_\perp}$ given in SRun is not used. The BLS900 is a scintillometer with two transmitters and one receiver. Raw signal intensities were measured and stored at a frequency of 500 Hz. The setup of the scintillometer is the same as that of other recent Helsinki scintillometer work (Wood et al., 2013b). The scintillometer measured over a path of 4.2 km. The transmitter unit was placed at a height of 67 m, while the receiver was placed at a height of 52.9 m (see Fig. 1). The orientation of the scintillometer was ~~near north–south-axis~~ nearly north–south (17°) – therefore, the wind was near-perpendicular to the scintillometer path when it was blowing from the east or west. In this study, $U_\perp$ is defined as positive when the wind is blowing from the west into the path.

The Doppler lidar was placed near the receiver of the scintillometer at a height of 45 m. Each ray lasts for 1 s and is repeated ~~each~~ every 4 s. Every 5 min, a set of 10 rays (i.e., taking 40 s) was made comprising different beam angles. From this set, only the 174 and 196°azimuth angles were used in this study, see Fig. 1. This pair was wider apart than desired, due to line-of-sight issues~~which are typical for urban environments~~. The elevation of the beam was 0.45°. The Doppler lidar data are given in a series of 30-m range-gates centered ~~from~~ at distances 105–9585 m from the instrument, but data were only needed until ~~4095~~4155 m (i.e., 139 range-gates corresponding to the length of the scintillometer path). However – given the atmospheric aerosol loading, sensitivity of the instrument, and integration times – sometimes not enough signal ~~can be~~ could returned from the farthest gates and therefore results in a limited range of the data. In order to compare the Doppler lidar ~~measurements~~ estimates with $\overline{U_\perp}$ ~~measurements~~ estimates of the scintillometer, two of the Doppler lidar ~~scans~~ estimates were averaged. Therefore, $\overline{U_\perp}$ ~~measurements~~ estimates of the Doppler lidar were available at 10-minute intervals.

A 3D sonic anemometer was located at 75 m height (near the scintillometer transmitter unit at Hotel Torni, denoted here as "Anemometer south") and another at 60 m (near the receiver at the so-called SMEAR-III-Kumpula station, denoted here as "Anemometer north"), see Fig. 1. Due to the mast mounting, the wind directions are more uncertain for 0–50°for Anemometer north, and in between 50–185°for Anemometer south. Fortunately, the wind directions during the study were mainly 210–350°. For more details of the anemometer setup see Järvi et al. (2009) and Nordbo et al. (2013). The value of $U_\perp$ measured by each of the ~~anemometer~~ anemometers was added to the beginning and the end of the Doppler lidar-path ~~measurements~~estimates, giving a fuller path of $U_\perp(x)$. The ~~measurements~~ estimates of $U_\perp(x)$ were path-averaged according to the scintillometer path-weighting function given by Wang et al. (1978) for comparison with $\overline{U_\perp}$ ~~measured~~ estimated by the scintillometer. In case of missing $U_\perp(x)$ data the path-weighting factors were scaled to a total of 100 % in order to calculate the estimate of $\overline{U_\perp}$ of the Doppler lidar. Note that because of the bell-shaped path-weighting function, the anemometer measurements are barely (only for 2.5 %) included in the ~~weight-averaged~~ path-weight averaged $U_\perp$ ~~measurements~~ estimates over the path. For the comparison between Doppler lidar and scintillometer, an arbitrary requirement was that at least 50 % of $U_\perp(x)$ of the Doppler lidar data were available along the ~~first 139 range-gates (i.e., corresponding to the scintillometer path)~~scintillometer path.

4 Results and discussion

4.1 Doppler lidar path-resolved crosswinds

For the Doppler lidar, the urban environment is challenging, since the duo-beam method assumes a homogeneous wind field at each range-gate distance. This assumption will be violated to an unknown degree as the pair of beams diverges. Therefore– before comparing the scintillometer with the Doppler ~~lidar,~~ lidar– measurements periods and conditions are identified where the Doppler lidar differs from south anemometer measurements. We evaluate the difference between $U_\perp(x)$ ~~measured~~ estimated by the Doppler lidar and $U_\perp$ measured by the south anemometer, to see the impact of the wind direction and building height (see Fig. 2). Note that a perfect agreement between the Doppler lidar and anemometer ~~measurements~~ estimates is not expected, since the measurement locations are different. The first ten

range-gates of $U_\perp$ of the Doppler lidar compared well with that measured by anemometer north for the time-period studied, with root-mean-square error (RMSE) values of 0.57 m s^{-1}. Hirsikko et al. (2014) showed for the same experimental setup, but a different time-period, a RMSE of 0.53–0.67 m s^{-1} for the Doppler velocity between Doppler lidar and sonic anemometer.

It should be noted that the sign of $U_\perp(x)$ is determined by the wind direction estimated by the Doppler lidar. When the wind is near parallel to the path, a small ~~change in~~ error in the estimated wind direction can result in ~~a sign change~~ an error of the sign of $U_\perp(x)$. ~~However, in general the $U_\perp$-values are reasonably low in these conditions.~~ The wind directions where the wind is near-parallel to the path (167–227°and 347–47°) are denoted in light-red shading in the lower figure-panel. It can clearly be seen that there is a substantial difference between Doppler lidar and anemometer for these wind directions, especially when the wind is blowing from 200–227°. Even sign changes of the difference are observed. ~~Besides being parallel to the path, the~~ The winds from the 200–227°directions are also strong ($>$ 5 m s^{-1}). Therefore, ~~besides being parallel to the path,~~ the corresponding $U_\perp(x)$-values are still moderate (absolute up to 3 m s^{-1}) for these wind directions. A small error in the wind direction can therefore result in a sign change of a moderate $U_\perp(x)$, which is indeed what we see in Fig. 2. Also for the wind direction 347–46°there is a clear difference between $U_\perp(x)$ of the Doppler lidar and $U_\perp$ of the anemometer, with ~~values~~ differences up to 10 m s^{-1}. Whilst we might expect differences in the roughness sublayer, to have such large differences for hundreds of meters seems unrealistic. Perhaps this is a breakdown of the homogeneity assumption required for the duo-beam method. Whatever the cause, it is deemed that Doppler lidar values where the wind direction is 167–227°and 347–46°are excluded for the rest of the study (also ~~even~~ when selecting the four cases).

The difference between Doppler lidar and anemometer $U_\perp$ is also large from 2000–2500 m along the Doppler lidar path (indicated in light red in Fig. 2 on the right). This is probably caused by differences in the wind fields measured by the two beams, since the ~~large divergence between the beams, especially when the~~ 196°-beam passes near to a high church tower (Kallio, about 93 m asl) which is located ~~at around~~ 35 m from the 196°-beam and at 2300 m distance ~~.~~ from the Doppler lidar (see Fig. 1b). Although the church tower is somewhat to the east of the Doppler lidar path it ~~has apparently also~~ apparently has a significant influence on the wind-field ~~measured~~ estimated by the Doppler lidar. The church ~~creates heterogeneity in the wind-field~~ alters the wind field of one of the Doppler lidar path (196°),

while the other beam (174°) does not encounter this alteration. Thus, the wind field sampled by the two Doppler lidar beams are not homogeneous, which causes problems for the duo-beam method. Therefore, we also excluded $U_\perp(x)$-values ~~measured~~ estimated by the Doppler lidar from 2000–2500 m for the ~~validation of scintillometer measurements~~ evaluation of scintillometer estimates with Doppler lidar ~~measurements~~estimates. However, in order to evaluate the response of a variable $U_\perp(x)$ on $S_{11}(f)$ and $r_{12}(\tau)$, and thereby on $\overline{U_\perp}$ ~~measured~~ estimated by the scintillometer, the four selected cases need the complete $U_\perp(x)$ of the scintillometer path. Therefore, when selecting the four cases the value of $U_\perp(x)$ had to be below $1.5 \cdot \overline{U_\perp}$ (of the Doppler lidar estimates) for 2000 m $\leq x \leq$ 2500 m.
Although, the data where the wind direction was 167–227°or 347–46°are excluded, as are the data 2000–2500 m along the Doppler lidar path, there are still enough data-points left for the comparison between Doppler lidar and scintillometer. ~~To be included in the comparison at least 50 % of $U_\perp(x)$ had to be present in the Doppler lidar data. This~~ The exclusion resulted in 1288 10-min data-points (60 % of the data) for the comparison between Doppler lidar and scintillometer. For the four cases, the complete scintillometer path had to be covered by the Doppler lidar. The four cases selected are indicated in Fig. 2. These cases are spread over the measurement period, and have different $\overline{U_\perp}$ values. In order to smooth the Doppler lidar data slightly, a moving average of 5 points was applied to $U_\perp(x)$. The results of the four cases are presented in Sect. 4.3.

4.2 Path-averaged crosswinds

In this section, $\overline{U_\perp}$ obtained by the scintillometer ~~are~~ is compared to that of the Doppler lidar. Note that the scintillometer path and the Doppler lidar duo-beam setup are not ~~measuring exactly the same atmosphere~~ sampling the same part of the atmosphere exactly (see Fig. 1). Therefore, a perfect one-to-one correlation cannot be expected. ~~The theoretical difference between $\overline{U_\perp}$ obtained by~~ However, the height difference between the scintillometer and ~~Doppler lidar (given their difference in heights) can be approximated by assuming a horizontally homogeneous neutral wind-profile, knowing the beam heights along the paths (excluding the 2000–2500 m of the path), and using the path-weighting averaging of the scintillometer. For this setup the scintillometer would overestimate~~ the Doppler lidar beam causes a negligible difference in the $\overline{U_\perp}$ ~~compared to the Doppler lidar by a mere~~ estimates. Assuming a neutral wind profile the difference in $\overline{U_\perp}$ is merely 1.1 ~~%~~% (with a higher $\overline{U_\perp}$

estimate of the scintillometer), which assures that the height difference between the two measurement devices should not influence the comparison. Note that this ~~theoretical difference is only done to get an idea of how strong the comparison between the Doppler lidar and scintillometer are affected by the difference in height between the two beams~~1.1 % is only an approximation, in reality ~~it~~ the comparison is more complicated since part of the measurements are done in the roughness sublayer where logarithmic wind profiles are not applicable. ~~In theory the difference between the two measurement techniques should be less in unstable conditions, while in stable conditions the difference should be more. For the scintillometer, the cumulative spectrum method (based on $S_{11}(f)$) and the lookup table method (based on $r_{12}(\tau)$) are used. The results are presented in Fig 3.~~

We first focus on the result of the cumulative spectrum method (Fig. 3a). Note that the plots in Fig. 3 are colored with the standard deviation path-averaged by the scintillometer path-weighting function ($\overline{\mathrm{STD}_{\mathrm{U}\perp}}$, i.e., fluctuations of $U_\perp(x)$ in the middle of the path contribute more to $\overline{\mathrm{STD}_{\mathrm{U}\perp}}$ than those at the ends of the path). Recall that the sign of $\overline{U_\perp}$ is unknown with the cumulative spectrum method, and thus the absolute values of $\overline{U_\perp}$ are compared to each other. There is a reasonable correlation between $\overline{U_\perp}$ of the scintillometer and Doppler lidar, with an RMSE of 0.73 m s^{-1}. However, for higher path-weighted standard deviation along the scintillometer path ($\overline{\mathrm{STD}_{\mathrm{U}\perp}}$), more scatter occurs between the scintillometer and Doppler lidar ~~measurements~~estimates. Only taking into account the data points where $\overline{\mathrm{STD}_{\mathrm{U}\perp}} > 2$ m s^{-1} leads to an R^2 value of 0.32 and an RMSE of 0.86 m s^{-1}. This higher scatter when $\overline{\mathrm{STD}_{\mathrm{U}\perp}} > 2$ m s^{-1}, indicates the difficulty ~~in~~ of obtaining $\overline{U_\perp}$ when the wind field is more variable along the path. An RMSE of 0.73 m s^{-1} is ~~reasonably~~ low. For measurements in London (Wood et al., 2013c) for comparable wind conditions, horizontal wind speed RMSEs were found of 0.35 m s^{-1} between two sonic anemometers on the same mast, 0.71–0.73 m s^{-1} between two sonic anemometers on different masts, 0.65–0.68 ~~m s^{-1}~~ m s^{-1} between Doppler lidar and sonic anemometers. And for $\overline{U_\perp}$, Wood et al. (2013c) showed, an RMSE of 1.12–2.13 m s^{-1} between scintillometer and Doppler lidar. For a flat grassland site, where $U_\perp(x)$ can be assumed to be rather homogenous, van Dinther et al. (2013) and van Dinther and Hartogensis (2014) showed RMSE values of ~~quality checked~~ quality-checked data of 0.41–0.67 m s^{-1} between a scintillometer and sonic anemometer for similar $\overline{U_\perp}$-conditions (in absolute values is between 0 and 6 m s^{-1}. Therefore, we can conclude, that despite the higher scatter for variable $U_\perp(x)$-conditions, both measurement techniques seem able to obtain $\overline{U_\perp}$ in this challenging environment.

In Fig. 3b, $\overline{U_\perp}$ obtained by the lookup table method is compared to the Doppler lidar ~~measurements.~~ estimates. Note that the following regression statistics are obtained when absolute $\overline{U_\perp}$-values are considered for the lookup table method: RMSE of 0.73 m s^{-1}, $y = 0.76x + 0.83$, and $R^2 = 0.53$ Just like the cumulative spectrum method, there is a clear correlation between $\overline{U_\perp}$ ~~measured~~ estimated by the scintillometer and that ~~measured~~ estimated by the Doppler lidar. ~~The RMSE is for the lookup table method slightly lower (0.71 m s^{-1}) than that of the cumulative spectrum with the Doppler lidar. The lookup table method also yields the sign of~~ Considering the regression statistics of the absolute $\overline{U_\perp}$ ~~(here only four points). Besides having a lower RMSE , the fit of $\overline{U\perp}$ of~~ are very similar with the same RMSE and similar regression equation (slightly better fit for the lookup table method~~with the Doppler lidar is better than that of cumulative spectrum method. This better fit is clearly visible by the regression equations; with a slope closer to one (0.79 compared to 0.71)and a lower offset (0.79 compared to 0.97~~). The scatter of $\overline{U_\perp}$ of the lookup table method with the Doppler lidar ~~measurements are also~~ estimates is somewhat lower than that of the cumulative spectrum method with an R^2-value of ~~0.56~~ 0.53 compared to 0.47. For the lookup table, the scatter is also higher (R^2 of 0.37 and RMSE of 0.88 m s^{-1}) when $U_\perp(x)$ is very variable ($\overline{\mathrm{STD}_{\mathrm{U}\perp}} > 2$ m s^{-1}).
Overall, both scintillometer methods are able to obtain a similar $\overline{U_\perp}$ as the Doppler lidar. This indicates that both the Doppler lidar and scintillometer are able to obtain $\overline{U_\perp}$ over the complex urban environment. However, bear in mind that in order to achieve these results certain wind directions and a certain section of the path were not take into account (see Section 4.1). The lookup table method showed the best results, with the lowest RMSE and scatter.

4.3 Variable crosswinds along the path

Four cases were selected to investigate the influence of a variable $U_\perp(x)$ on $S_{11}(f)$ and $r_{12}(\tau)$; A, B, C, and D (see top panels Fig. 4 and Table 1). As a measure of the variability of $U_\perp(x)$, the weight-averaged standard deviation of $U_\perp(x)$ is normalized by $\overline{U_\perp}$ ($\overline{\mathrm{STD}_{\mathrm{U}\perp*}}$). For case B and D, $\overline{U_\perp}$ is ~~reasonably high~~ moderate with a $\overline{U_\perp}$ of 3.3 and 3.9 m s^{-1} respectively. The variability of $U_\perp(x)$ is similar for both cases, with reasonable high values for $\overline{\mathrm{STD}_{\mathrm{U}\perp*}}$ of 0.39–0.41. For case C, $\overline{U_\perp}$ is reasonably low with a $\overline{U_\perp}$ of 1.6 m s^{-1}. Although $\overline{U_\perp}$ is low, the variability of $U_\perp(x)$ is high with a value of $\overline{\mathrm{STD}_{\mathrm{U}\perp*}}$ of 0.63. For case A, $\overline{U_\perp}$ is moderate with a value of 2.8 m s^{-1}. The variability of $U_\perp(x)$ is moderate, with a $\overline{\mathrm{STD}_{\mathrm{U}\perp*}}$ of 0.36. For these four

cases, the theoretical $S_{11}(f)$ and $r_{12}(\tau)$ are calculated using Eq. (1) and Eq. (3), respectively. ~~Results are presented in Fig. 4.~~

We first focus on the ~~results of the~~ cumulative scintillation spectra (CS, given in the middle panels of Fig. 4). Remember that the cumulative spectrum method determines $\overline{U_\perp}$ from the frequencies where the CS is 0.5, 0.6, 0.7, 0.8, and 0.9. Therefore, in Fig. 4 the cumulative spectra are zoomed into these points. For simplicity we abbreviate the cumulative spectrum obtained from the scintillometer as $\mathrm{CS_{scint}}$, the cumulative spectrum obtained from Eq. (1) using $U_\perp(x)$ of the Doppler lidar as $\mathrm{CS_{varU\perp}}$, and the cumulative spectrum obtained from Eq. (1) using $\overline{U_\perp}$ of the Doppler lidar as $\mathrm{CS_{constU\perp}}$. ~~We first focus on the results of the cumulative scintillation spectra (CS, given in the middle panels of Fig. 4).~~

There is a difference between $\mathrm{CS_{varU\perp}}$ and $\mathrm{CS_{constU\perp}}$ for all four cases. Therefore, the CS is indeed influenced by a variable $U_\perp(x)$ as was suggested by van Dinther et al. (2013). Recall that when a ~~CS-points~~ CS-point shifts to a higher frequency, the retrieved value of $\overline{U_\perp}$ will be higher; and the other way around (see Eq. (2)). The CS-points of 0.5, 0.6, and 0.7 lie at lower frequencies for $\mathrm{CS_{varU\perp}}$ than for $\mathrm{CS_{constU\perp}}$, while the 0.9 CS-point lies at higher frequencies. $\mathrm{CS_{scint}}$ is more similar to $\mathrm{CS_{varU\perp}}$ than to $\mathrm{CS_{constU\perp}}$, which indicates that Eq. (1) is also applicable when $U_\perp(x)$ is variable.

The results of applying the cumulative spectrum method to $\mathrm{CS_{scint}}$ and $\mathrm{CS_{varU\perp}}$ are given in Table 1. If the assumption of the cumulative spectrum methods, that C_{CS} of Eq. (2) is constant, ~~holds also~~ also holds for variable $U_\perp(x)$, then the value of $\overline{U_\perp}$ of the Doppler lidar should be identical to that of $\overline{U_{\mathrm{CSvarU\perp}}}$. For case D this is indeed ~~the case.~~ true.

However, for case A, B, and C $\overline{U_{\mathrm{CSvarU\perp}}}$ is 0.2 m s^{-1} lower than $\overline{U_{\mathrm{Lidar}}}$. Therefore, the assumption that C_{CS} is constant does not hold. However, the error that is made in $\overline{U_\perp}$ is reasonably small (0.2 m s^{-1}). This small error is due to the fact that the cumulative spectrum method calculates $\overline{U_\perp}$ for five frequency points and then averages these to obtain one value for $\overline{U_\perp}$ (see Sect. 2.1.1). For the 0.5, 0.6, and 0.7 CS-point, $\overline{U_{\mathrm{CSvarU\perp}}}$ is underestimated, while for the 0.9 CS-point $\overline{U_{\mathrm{CSvarU\perp}}}$ is overestimated. Therefore, applying a method with only one frequency point to obtain $\overline{U_\perp}$ is more likely to have a higher error. This makes the cumulative spectrum method the most suitable method to obtain $\overline{U_\perp}$ from $S_{11}(f)$ when $U_\perp(x)$ is variable, compared to other methods suggested by van Dinther et al. (2013). Alternatively, to obtain $\overline{U_\perp}$ even more reliably from $S_{11}(f)$ in variable $U_\perp(x)$ conditions, an approach similar to the lookup table method can be applied. A lookup table can be created of the theoretical CS for different $\overline{U_\perp}$-values and also different variabilities of $U_\perp(x)$.

Next we focus on the results of the lookup table method, which relies on $r_{12}(\tau)$ to obtain $\overline{U_\perp}$ (given in the bottom panels of Fig. 4). What stands out is that for all cases, except case B, there is a substantial difference in magnitude between $r_{12\ \mathrm{varU}\perp}(\tau)$ (grey solid lines) and $r_{12\ \mathrm{constU}\perp}(\tau)$ (grey dotted lines). However, the magnitude of $r_{12}(\tau)$ does not influence $\overline{U_\perp}$ obtained by the lookup table method, but the shape of $r_{12}(\tau)$ does. The shape of $r_{12}(\tau)$ also changes when $U_\perp(x)$ is variable: it becomes wider. For all four cases $r_{12\ \mathrm{varU}\perp}(\tau)$ resembles $r_{12\ \mathrm{scint}}(\tau)$ better than $r_{12\ \mathrm{constU}\perp}(\tau)$. This resemblance indicates that the theoretical model of Lawrence et al. (1972) (Eq. (3)) can be used to obtain $r_{12}(\tau)$ also given a variable $U_\perp(x)$. The fact that variable $U_\perp(x)$ causes a wider $r_{12}(\tau)$ can cause an underestimation of $\overline{U_\perp}$ obtained by the scintillometer, since low $\overline{U_\perp}$ values cause high r_{12}-values at high τ values. For the four cases selected in this study $\overline{U_\perp}$ calculated from $r_{12\ \mathrm{varU}\perp}$ is indeed ~~too low~~ lower than $\overline{U_\perp}$ estimated by the Doppler lidar (see Table 1). The error is in this study defined as the difference between $\overline{U_\perp}$ estimated by the Doppler lidar and $\overline{U_\perp}$ obtained from $r_{12}(\tau)$. For case C and D the error is reasonably high with a value of 0.8 m s^{-1}. This high error is caused by the fact that for these two cases $r_{12}(\tau)$ is not only lowered by the variable $U_\perp(x)$, but the peak in $r_{12}(\tau)$ also changes location and $r_{12}(\tau)$ becomes much wider due to the variable $U_\perp(x)$. For these cases $\overline{\mathrm{STD}_{\mathrm{U}\perp *}}$ is also high with values of 0.63 and 0.41, respectively. Although the error with the Doppler lidar ~~measurements~~ estimates is high for case C and D, the ~~measured~~ estimated $\overline{U_{\perp\mathrm{scint}}}$ of the lookup table method are for these cases exactly identical to that of $r_{12\mathrm{varU}\perp}(\tau)$. Therefore, ~~by~~ if the lookup table was expanded to also including variable $U_\perp(x)$ ~~in the~~ field the results of the lookup table method ~~the results of this method~~ in a more challenging environment ~~can~~ could be improved. The underestimation of $\overline{U_\perp}$ given in the cases is however not clearly visible in the comparison Doppler lidar and scintillometer (see Sect. 4.2 Fig. 3). Although, we do see that a higher $\overline{\mathrm{STD}_{\mathrm{U}\perp}}$ causes more scatter between $\overline{U_\perp}$ of the scintillometer and Doppler lidar.

From the analysis of these four cases, it follows that the present cumulative spectrum method is better equipped to obtain $\overline{U_\perp}$ than the lookup table method. However, as mentioned before the lookup table method can be adjusted to ~~also~~ take into account the variability of $U_\perp(x)$. The underestimation of $\overline{U_\perp}$ found for the four cases for both methods was not clearly distinguishable in Sect. 4.2. Though more scatter occurred between $\overline{U_\perp}$ ~~measured~~ estimated by scintillometer and Doppler lidar when $\overline{\mathrm{STD}_{\mathrm{U}\perp}}$ was high ($>$ 2 m s^{-1}).

5 Conclusions

In this study, ~~measurements~~ estimates of $U_\perp$ above the urban environment of Helsinki from sonic anemometers and Doppler lidar data were compared with scintillometer data. The anemometers measured at either ends of the scintillometer path, and the Doppler lidar was ~~pointed horizontally along~~ measuring alongside the scintillometer path. For the Doppler lidar duo-beam method, sign problems of $U_\perp$ naturally occurred when the wind direction was ~~perpendicular~~ parallel to the scintillometer path (167–227°and 347–47°). In the middle of the path (2000–2500 m) a church tower near one of the Doppler lidar beams resulted in problems, presumably because of the heterogeneity it introduced in the wind field. Therefore, for the comparison with the scintillometer these points were excluded.

For the scintillometer, two different methods were tested: the cumulative spectrum method (van Dinther et al., 2013), based on $S_{11}(f)$, and the lookup table method (van Dinther and Hartogensis, 2014), based on $r_{12}(\tau)$). Both methods gave similar results as the Doppler lidar ~~measurements, albeit~~ estimates, although with scatter between the Doppler lidar and the scintillometer (especially for conditions where $\overline{\mathrm{STD}_{\mathrm{U}\perp}} > 2$ m s^{-1}). Still, given that the Doppler lidar and scintillometer did not sample the exact same area in this urban environment, the good fit and low RMSE (≤ 0.73 m s^{-1}) ~~indicates~~ indicate that both measurement devices are able to obtain $\overline{U_\perp}$, given the data treatment applied in this study,. For the scintillometer the method relying on $r_{12}(\tau)$ (lookup table method) is preferable, since $r_{12}(\tau)$ is determinable over short time scale ($\sim$ 10 s) compared to scintillation spectra ($\sim$ 10 min) and it also includes information about the sign of $\overline{U_\perp}$.

Four cases were selected to investigate the influence of a variable $U_\perp(x)$ on $\overline{U_\perp}$ ~~measured~~ estimated by the scintillometer. Variability of $U_\perp(x)$ causes only a slight difference between $\overline{U_\perp}$ obtained by the cumulative spectrum method and Doppler lidar (error $\leq$ ~~−0.2~~0.2 m s^{-1}). $r_{12}(\tau)$ was more affected by a variable $U_\perp(x)$-field than $S_{11}(f)$ leading to higher errors in $\overline{U_\perp}$ obtained by the lookup table method (error $\leq$ ~~−0.8~~0.8 m s^{-1}). The lookup table method can ~~,~~ however, be adjusted ~~by also including~~ to include heterogeneous wind fields~~in the lookup table method~~; thereby, probably making the scintillometer more suitable to obtain $\overline{U_\perp}$ in a more challenging environment.

By applying two scintillometers with paths perpendicular to each other, not only $\overline{U_\perp}$ could be obtained, but also the wind direction and horizontal wind speed. Thereby, obtaining an area-averaged value of the horizontal wind speed and wind direction above an urban

environment. This would be directly useful for nowcasting for meteorology and for atmospheric composition (AC); and also in the development of models of AC and numerical weather prediction.

Acknowledgements. The authors would like to thank Leena Järvi, Rostislav Kouznetsov, Anne Hirsikko, and Ville Vakari for their help with instrumental setup and preliminary data analysis; and Kari Riikonen, Erkki Siivola, Petri Keronen, and Sami Haapanala for their technical support. Daniëlle van Dinther and Oscar Hartogensis were supported by the Knowledge for Climate project Theme 6 entitled ”“High Quality Climate Projections” (KVK-HS2). Curtis Wood was supported by the EC FP7 ERC Grant 227915 ”“Atmospheric planetary boundary layers: Physics, modelling and role in Earth system”.

References

Bornstein, R. D. and Johnson, D. S.: Urban–rural wind velocity differences, Atmospheric Environment, 11, 597–604, 1977.

Briggs, B. H., Phillips, G. J., and Shinn, D. H.: The Analysis of Observations on Spaced Receivers of the Fading of Radio Signals, Proceedings of the Physical Society B, 63, 106–121, 1950.

Clifford, S. F.: Temporal-frequency spectra for a spherical wave propagating through atmospheric turbulence, Journal of the Optical Society of America, 61, 1285–1292, 1971.

De Bruin, H.: Introduction: renaissance of scintillometry, Boundary-Layer Meteorology, 105, 1–4, 2002.

Hirsikko, A., O'Connor, E. J., Komppula, M., Korhonen, K., Pfüller, A., Giannakaki, E., Wood, C. R., Bauer-Pfundstein, M., Poikonen, A., Karppinen, T., Lonka, H., Kurri, M., Heinonen, J., Moisseev, D., Asmi, E., Aaltonen, V., Nordbo, A., Rodriguez, E., Lihavainen, H., Laaksonen, A., Lehtinen, K. E. J., Laurila, T., Petäjä, T., Kulmala, M., and Viisanen, Y.: Observing wind, aerosol particles, cloud and precipitation: Finland's new ground-based remote-sensing network, Atmospheric Measurement Techniques, 7, 1351–1375, 2014.

HSY: SeutuCD (CD-rom), 2008.

Järvi, L., Hannuniemi, H., Hussein, T., Junninen, H., Aalto, P., Hillamo, R., Mäkelä, T., Keronen, P., Siivola, E., Vesala, T., and Kulmala, M.: The urban measurement station

SMEAR III: Continuous monitoring of air pollution and surface–atmosphere interactions in Helsinki, Finland., Boreal Environmental Research, 14, 86–109, 2009.

Kolmogorov, A. N.: The local structure of turbulence in an incompressible viscous fluid for very large Reynolds numbers, Doklady Akademii Nauk SSSR, 30, 299–303, 1941.

Lawrence, R. S., Ochs, G. R., and Clifford, S. F.: Use of scintillations to measure average wind across a light beam., Applied Optics, 11, 239–43, 1972.

Meijninger, W. M. L., Green, A. E., Hartogensis, O. K., Kohsiek, W., Hoedjes, J. C. B., Zuurbier, R. M., and De Bruin, H. A. R.: Determination of area-averaged water vapour fluxes with large aperture and radio wave scintillometers over a heterogeneous surface – Flevoland Field Experiment, Boundary-Layer Meteorology, 105, 63–83, 2002a.

Meijninger, W. M. L., Hartogensis, O. K., Kohsiek, W., Hoedjes, J. C. B., Zuurbier, R. M., and De Bruin, H. A. R.: Determination of area-averaged sensible heat fluxes with a large aperture scintillometer over a heterogeneous surface – Flevoland field experiment, Boundary-Layer Meteorology, 105, 37–62, 2002b.

Nieveen, J. P., Green, A. E., and Kohsiek, W.: Using a large-aperture scintillometer to measure absorption and refractive index fluctuations, Boundary-Layer Meteorology, 87, 101–116, 1998.

Nordbo, A., Järvi, L., Haapanala, S., Moilanen, J., and Vesala, T.: Intra-City Variation in Urban Morphology and Turbulence Structure in Helsinki, Finland, Boundary-Layer Meteorology, 146, 469–496, 2013.

PaITuli: Topographic Dataset of National Land Survey of Finland, https://sui.csc.fi/applications/paituli/infra.html, 2012.

Poggio, L. P., Furger, M., Prévôt, A. H., Graber, W. K., and Andreas, E. L.: Scintillometer Wind Measurements over Complex Terrain, Journal of Atmospheric and Oceanic Technology, 17, 17–26, 2000.

van Dinther, D. and Hartogensis, O. K.: Using the Time-Lag-Correlation function of Dual-Aperture-Scintillometer measurements to obtain the Crosswind, Journal of Atmospheric and Oceanic Technology, 31, 62–78, 2014.

van Dinther, D., Hartogensis, O. K., and Moene, A. F.: Crosswinds from a Single-Aperture Scintillometer Using Spectral Techniques, Journal of Atmospheric and Oceanic Technology, 30, 3–21, 2013.

Wang, T., Ochs, G. R., and Clifford, S. F.: A saturation-resistant optical scintillometer to measure C_{n^2}, Journal of the Optical Society of America, 68, 334–338, 1978.

Wang, T. I., Ochs, G. R., and Lawrence, R. S.: Wind measurements by the temporal cross-correlation of the optical scintillations., Applied Optics, 20, 4073–81, 1981.

Ward, H. C., Evans, J. G., and Grimmond, C. S. B.: Effects of Non-Uniform Crosswind Fields on Scintillometry Measurements, Boundary-Layer Meteorology, 141, 143–163, 2011.

Wood, C. R., Järvi, L., Kouznetsov, R. D., Nordbo, A., Joffre, S., Drebs, A., Vihma, T., Hirsikko, A., Suomi, I., Fortelius, C., O'Connor, E., Moiseev, D., Haapanala, S., Moilanen, J., Kangas, M., Karppinen, A., Vesala, T., and Kukkonen, J.: An Overview of the Urban Boundary Layer Atmosphere Network in Helsinki, Bulletin of the American Meteorological Society, 94, 1675–1690, 2013a.

Wood, C. R., Kouznetsov, R. D., Gierens, R., Nordbo, A., Järvi, L., Kallistratova, M. A., and Kukkonen, J.: On the Temperature Structure Parameter and Sensible Heat Flux over Helsinki from Sonic Anemometry and Scintillometry., Journal of Atmospheric and Oceanic Technology, 14, 1604–1615, 2013b.

Wood, C. R., Pauscher, L., Ward, H. C., Kotthaus, S., Barlow, J. F., Gouvea, M., Lane, S. E., and Grimmond, C. S. B.: Wind observations above an urban river using a new lidar technique, scintillometry and anemometry., Science of the Total Environment, 442, 527–33, 2013c.

Table 1. Crosswind for the four cases ~~measured~~ estimated by the Doppler lidar, and scintillometer (using either cumulative spectra, CS, or time-lagged correlation function, $r_{12}(\tau)$). $\overline{U_{\perp \mathrm{varU}\perp}}$ is given by the theoretical CS and $r_{12}(\tau)$ using the variable $U_{\perp}(x)$ ~~measured~~ estimated by the Doppler lidar.

Case	DOY	HH:MM (UTC)	Doppler lidar		CS		$r_{12}(\tau)$	
			$\overline{U_{\perp}}$	$\overline{\mathrm{STD}_{\mathrm{U}\perp *}}$	$\overline{U_{\mathrm{scint}}}$	$\overline{U_{\mathrm{varU}\perp}}$	$\overline{U_{\mathrm{scint}}}$	$\overline{U_{\mathrm{varU}\perp}}$
A	276	19:47	2.8	0.36	3.5	2.6	3.2	2.5
B	280	06:57	3.3	0.39	3.4	3.1	4.1	3.0
C	283	22:57	1.6	0.63	1.6	1.4	0.8	0.8
D	286	04:27	3.9	0.41	3.5	3.9	3.1	3.1

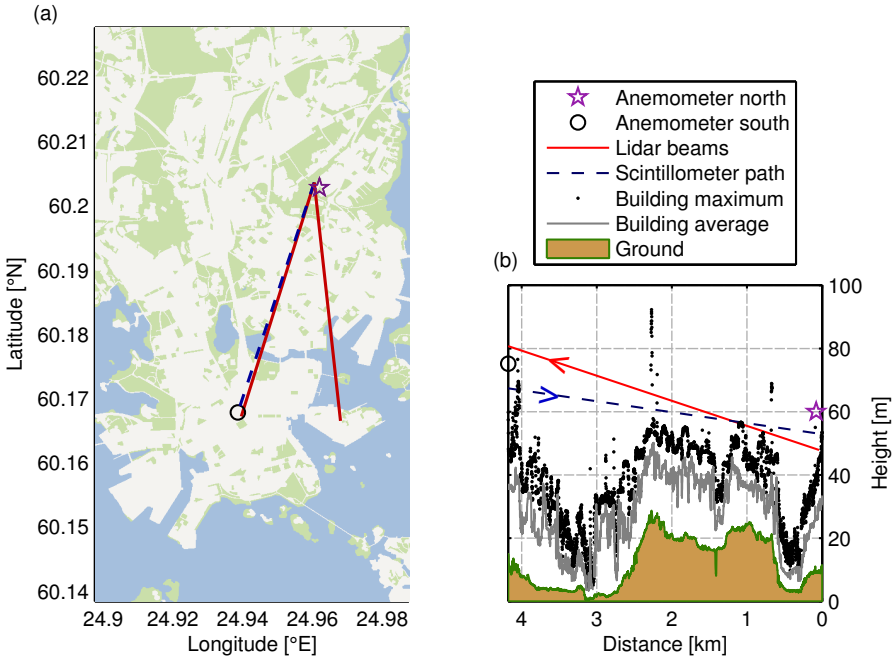

Fig. 1. (a) Experimental setup with the locations of the instruments in Helsinki indicated, including Doppler lidar-beam azimuths of 174 and 196°; shading is buildings/roads (white), grass/trees (green), and water (blue) (land cover data-source: HSY, 2008); the city-center is roughly the lower half of the map area. (b) A cross-section (height m asl) of the scintillometer beam and Doppler lidar 196°-beam; ~~building~~ average building height and maximum building height are with respect to ±250 m laterally of the 196°-beam (building height data source: PalTuli, 2012).

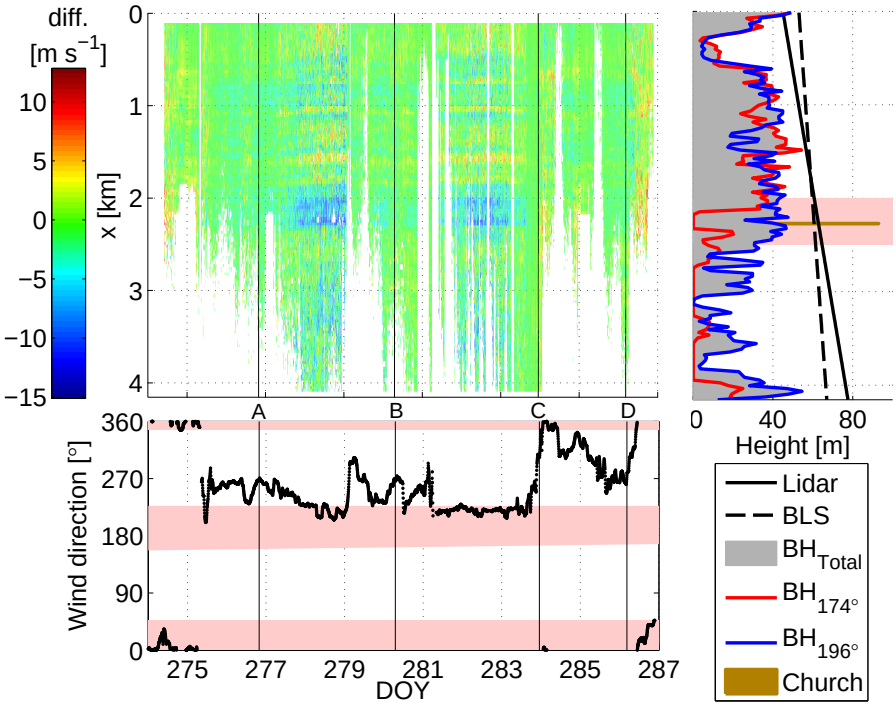

Fig. 2. The upper left panel shows the difference in $U_\perp$ ~~measured~~ estimated by the Doppler lidar duo-beam method compared with the south anemometer (colorbar) as a function of Doppler lidar beam distance (resolution of 30 m) and time (resolution of 10-min, DOY = day of year). The right panel shows the height (asl) of the Doppler lidar beam and building height (BH) $\pm$ 25 m laterally underneath the paths (total, and under beam with azimuth 174 and 196°). When there are no buildings below the path, BH indicates the height of highest ground point or zero when it is over sea. The lower panel shows wind direction against DOY from the south anemometer.

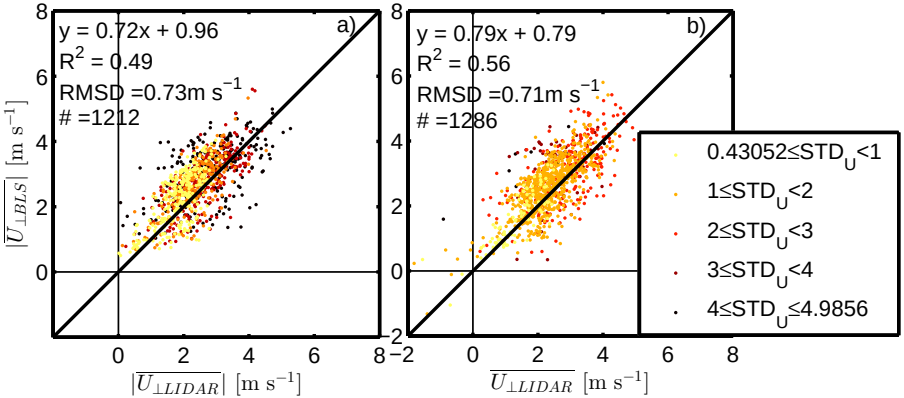

Fig. 3. (a) Crosswind ~~measured~~ 10-min averages estimated by the scintillometer ($\overline{U_{\perp\mathrm{Scint}}}$) using the cumulative spectrum method against Doppler lidar crosswind ($\overline{U_{\perp\mathrm{Lidar}}}$). (b) Crosswind ~~measured~~ estimated by the scintillometer using the lookup table method against Doppler lidar data. Both plots are color coded with the Doppler lidar-derived path weighted standard deviation of the crosswind along the 4.2 km path (~~colorbar on the right~~see legend). The one-to-one ~~line~~ lines are shown in thick black

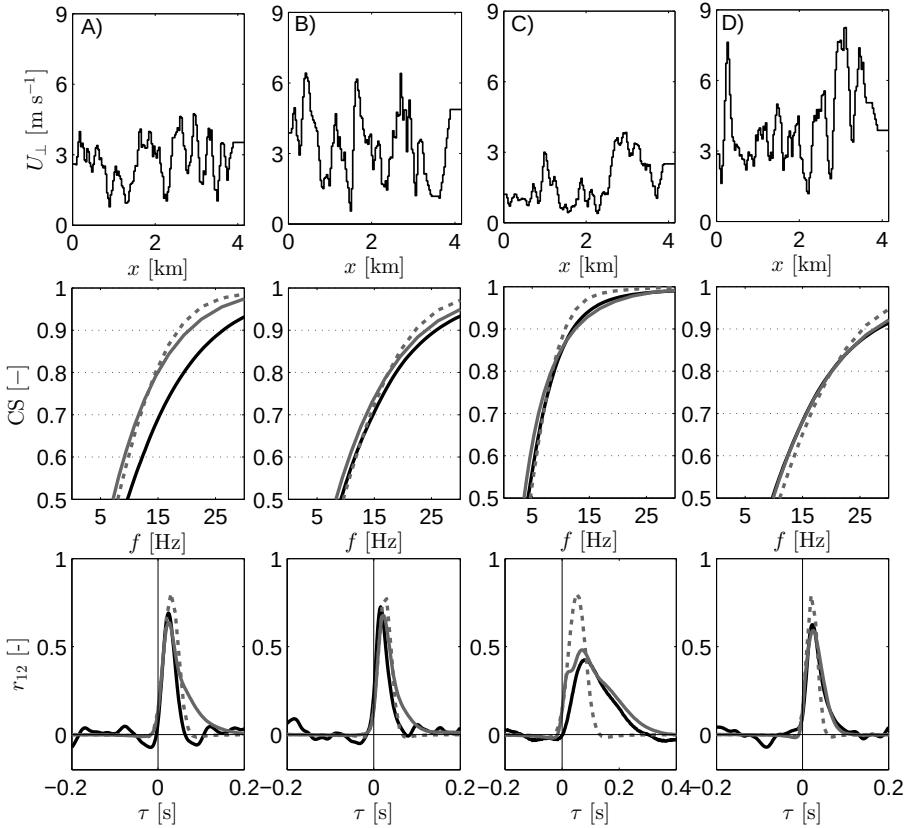
A)
B)
C)
D)
$U_\perp$ [m s^{-1}]
x [km]
CS [–]
f [Hz]
r_{12} [-]
τ [s]

Fig. 4. Four cases (A, B, C, and D) with in the top panels the transect of $U_\perp(x)$, in the middle panels the corresponding CS, and in the lower panels the corresponding $r_{12}(\tau)$. The ~~measured~~ estimated CS and $r_{12}(\tau)$ of the scintillometer are given in black solid lines, the theoretical CS and $r_{12}(\tau)$ given $U_\perp(x)$ of the Doppler lidar are given in solid grey lines, and the theoretical CS and $r_{12}(\tau)$ given $U_\perp(x) = \overline{U_\perp}$ are given in dashed grey lines.